Magnetic Resonance in Medicine 66:706–716 (2011)

Fast MR Parameter Mapping Using *k-t* Principal Component Analysis

Frederike H. Petzschner,[1–3]* Irene P. Ponce,[3] Martin Blaimer,[4] Peter M. Jakob,[3,4] and Felix A. Breuer[4]

Quantification of magnetic resonance parameters plays an increasingly important role in clinical applications, such as the detection and classification of neurodegenerative diseases. The major obstacle that remains for its widespread use in clinical routine is the long scanning times. Therefore, strategies that allow for significant decreases in scan time are highly desired. Recently, the *k-t* principal component analysis method was introduced for dynamic cardiac imaging to accelerate data acquisition. This is done by undersampling *k-t* space and constraining the reconstruction of the aliased data based on the *k-t* Broad-use Linear Acquisition Speed-up Technique (BLAST) concept and predetermined temporal basis functions. The objective of this study was to investigate whether the *k-t* principal component analysis concept can be adapted to parameter quantification, specifically allowing for significant acceleration of an inversion recovery fast imaging with steady state precession (TrueFISP) acquisition. We found that three basis functions and a single training data line in central *k*-space were sufficient to achieve up to an 8-fold acceleration of the quantification measurement. This allows for an estimation of relaxation times T_1 and T_2 and spin density in one slice with sub-millimeter in-plane resolution, in only 6 s. Our findings demonstrate that the *k-t* principal component analysis method is a potential candidate to bring the acquisition time for magnetic resonance parameter mapping to a clinically acceptable level. Magn Reson Med 66:706–716, 2011. © **2011 Wiley-Liss, Inc.**

Key words: *k-t* PCA; quantitative MRI; T_1-quantification; T_2-quantification; spin density quantification; relaxometry

INTRODUCTION

In recent years, quantitative parameter mapping in magnetic resonance imaging (MRI) has provoked interest as a promising approach in many clinical diagnostic applications (1), due to the fact that changes in tissue-dependent MR parameters can be indicative of changes in the tissue itself (2). Commonly used T_1 and T_2 weighted measurement techniques fail to provide statistically accessible information about absolute values of image intensities. Diagnosis therefore currently relies strongly on comparisons with surrounding tissue. MR parameter mapping, however, allows for a direct quantification of tissue dependent parameters. This has been shown to improve the early detection of diseases such as Parkinson's (3) and Alzheimer's disease (4) and also multiple sclerosis (5). Additional evidence of disease progression can be obtained by means of quantitative follow-up studies with these patients. Therefore, parameter measurements of the longitudinal relaxation time T_1, the transverse relaxation time T_2 and spin density can provide health care professionals with more information than current clinical protocols. This could result in shorter overall acquisition time for individual patients, improved diagnostic information and lower per person scanning costs.

The main reason why quantitative MR parameter mapping has not yet been established for widespread application in clinical diagnostics is the long scanning times; estimation of the MR parameters requires the acquisition of multiple images with various contrasts. Given the general trend in MRI towards higher spatial resolution in shorter acquisition times, fast quantification of the tissue-dependent parameters has also become the subject of extensive investigation (6). New acquisition techniques for parameter quantification have shortened the duration of whole brain quantification measurements down to 9 min for quantitative T_1 maps with 1 mm isotropic resolution (7). In addition, new combined acquisition approaches shortened the scanning time down to 17 min for T_1 and T_2 maps with 1mm isotropic resolution (8) or even 5 min for quantitative mapping of T_1, T_2, and PD and in-plane resolution of 0.8 and 5 mm slice thickness (9). The recently proposed inversion recovery (IR) TrueFISP sequence (10,11) allows for a simultaneous extraction of T_1, T_2 and relative spin density from a single experiment and therefore produces automatically registered and perfectly aligned parameter maps.

Long scanning times are also a problem in other MR imaging fields, such as dynamic imaging, where the acquisition of a series of images is required. Several studies on accelerated dynamic imaging propose acquisition schemes where the scanning time per image is shortened by undersampling *k*-space over time. This results in aliased signals, which can be resolved by various reconstruction methods such as TSENSE (12), TGRAPPA (13), *k-t* GRAPPA (14), *k-t* SENSE and *k-t* BLAST (15). The latter two use spatio-temporal correlations to reconstruct the missing data by an adaptive filtering process in *x-f*

[1]Neurological Research Center, Klinikum Grosshadern, Ludwig-Maximilians University Munich; Munich, Germany.
[2]Bernstein Center for Computational Neurosciences, Munich, Germany.
[3]Department of Experimental Physics 5, University of Würzburg, Würzburg, Germany.
[4]Research Center Magnetic Resonance Bavaria, Würzburg, Germany.
Grant sponsors: BayStMWIVT.
*Correspondence to: Frederike H. Petzschner, M.Sc. Hon., Ludwig-Maximilians University, Klinikum der Universität München, Neurologisches Forschungshaus, Marchioninistrasse 23, München 81377, Germany.
E-mail: fpetzschner@lrz.uni-muenchen.de
Received 25 June 2010; revised 17 December 2010; accepted 3 January 2011.
DOI 10.1002/mrm.22826
Published online 9 March 2011 in Wiley Online Library (wileyonlinelibrary.com).

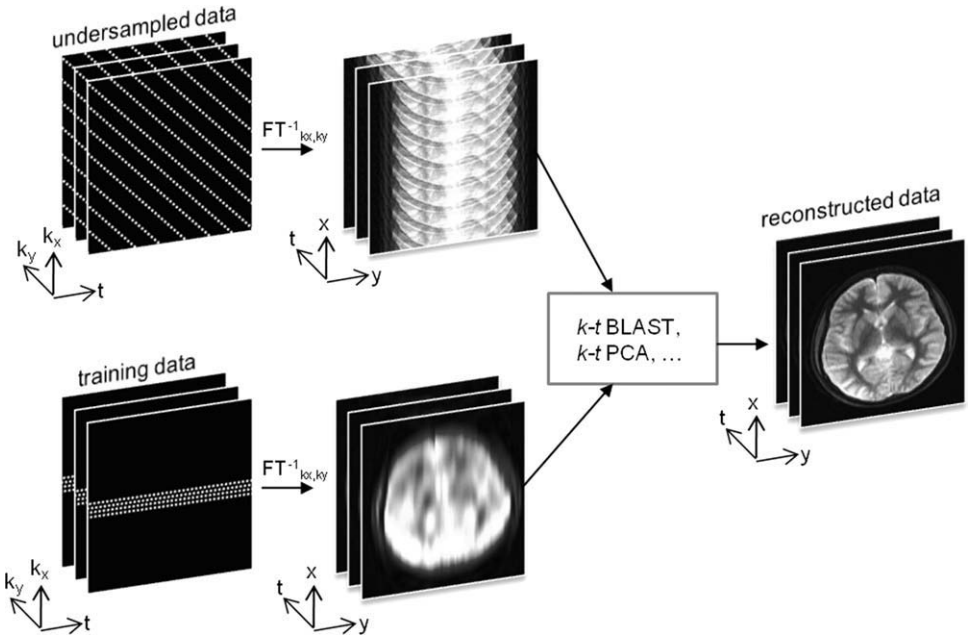

FIG. 1. Schematic overview of the acquisition scheme employed in *k-t* PCA and *k-t* BLAST. A set of training data and undersampled data in *k-t* space are acquired. For clarity, a representation of the data in the spatial domain is also given. The training data consist of only a few lines in central *k*-space fully sampled over time, leading to a high temporal but low spatial resolution. The undersampled data are shown for an 8× undersampled acquisition scheme according to a sheared grid, resulting in an aliased signal in the spatial domain.

space. They rely on the fact that cardiac data are restricted to a localized region in the *x-f* domain, i.e., there is a low degree of aliasing even in highly accelerated acquisitions. So far these techniques have not been proven applicable for MR parameter mapping, because the representation of these data in *x-f* space is less sparse, meaning there is a higher degrees of aliasing even at moderate acceleration rates. Yet, recently *k-t* PCA has been introduced as a generalization of the *k-t* BLAST method for dynamic imaging that is more suitable to resolve strong signal aliasing artifacts (16). The method uses a new set of temporal basis functions (principle components) obtained from training data, to reduce the number of degrees of freedom in the reconstruction. Thereby *k-t* PCA can better recover overlapping signals in an aliased object, if the number of basis functions is sufficiently low. This makes the *k-t* PCA method a promising candidate for reconstructing accelerated data sets that, like MR parameter mapping, have a high degree of aliasing in the *x-f* domain, but simple temporal dynamics.

The aim of this study was to investigate whether the *k-t* PCA method used in dynamic imaging can be successfully applied to significantly accelerate the acquisition of MR sequences for simultaneous acquisition of tissue-dependent parameters. We hypothesize that the temporal dynamics along an exponential relaxation curve can be described by only a very small number of basis functions. Hence the reconstruction of undersampled MR parameter data could be highly constrained. To demonstrate the potential benefits of this approach we applied the *k-t* PCA method to an IR TrueFISP acquisition sequence (10), thereby allowing for simultaneous quantification of T_1, T_2 and relative spin density in one slice with submillimeter in-plane resolution in only 6 s.

THEORY

Undersampled Acquisition

Dynamic imaging and MR parameter mapping require the acquisition of a series of images over time. Since most voxel intensities follow a specific temporal profile (e.g., cardiac motion), the *k-t* space data (k = reciprocal location, t = time) of these images series are highly correlated. To reduce redundancy and accelerate measurement time, new methods acquire a reduced amount of data over space and time (15,16) then using sophisticated reconstruction techniques to recover the entire image. Undersampling in the *k-t* domain, however, leads to a convolution of the true object signal with the point spread function in the reciprocal *x-f* space (x = location, f = frequency). If *k-t* space is sampled according to a lattice structure, the point spread function in the *x-f* space is also represented by a lattice structure. In this work, data are undersampled by a given acceleration factor (af) so that the acquired *k-t* sampling locations lie on a sheared grid (Fig. 1). The acceleration factor is defined as the number of phase encoding steps needed to reconstruct an alias-free image divided by the number of actually acquired phase-encoding lines per image. In the following sections, the mathematical principles of two techniques are presented that resolve the aliasing and reconstruct the true data, *k-t* BLAST and *k-t* PCA. Figure 2 provides an overview of the two methods, depicting both common and differing processing steps.

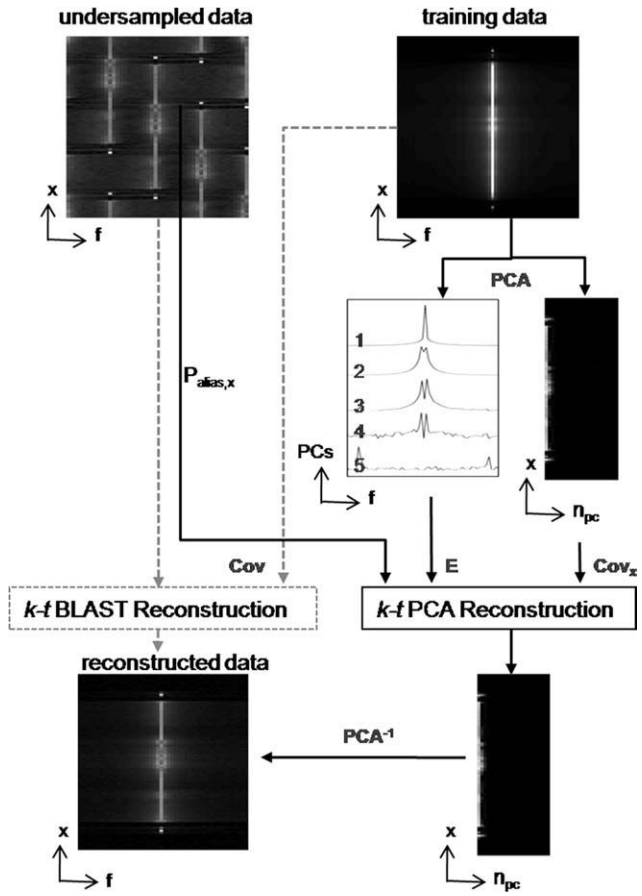

FIG. 2. Schematic overview of the *k-t* PCA procedure compared to *k-t* BLAST. Both methods use the representation of the training and undersampled data in the frequency domain for the data reconstruction. The *k-t* BLAST method relies solely on an estimate of the training covariance to resolve the aliasing in the undersampled data (dotted lines), while the *k-t* PCA concept performs a matrix factorization of the training data into a set of basis functions (principal components) to represent the data sparsely in a new basis set. In the case of *k-t* PCA, the aliasing is resolved for all temporal frequencies at once in the *x-pc* domain and finally, mapped back to the original basis in the *x-f* domain by the inverse PCA (solid lines).

k-t BLAST

According to the undersampling scheme the true object signals are mapped in such a way that they overlap in the corresponding *x-f* representation of the aliased data. The intensity of a single pixel in the aliased object at the location (x, f_m) is therefore composed of the interfering pixel intensities of the true object. In the case of 4-fold undersampling, for instance, the aliased signal can be expressed as the sum of four pixel intensities of the fully sampled object in the *x-f* domain

$$P_{\text{alias}}(x, f_m) = \mathbf{1}\begin{bmatrix} P_{xf}(x_1, f_{m,1}) \\ P_{xf}(x_2, f_{m,2}) \\ P_{xf}(x_3, f_{m,3}) \\ P_{xf}(x_4, f_{m,4}) \end{bmatrix} = \mathbf{1}\mathbf{P}_{\mathbf{xf}} \qquad [1]$$

where the measured pixel intensity is given by P_{alias} (x, f_m) and P_{xf} (x_i, $f_{m,i}$) denotes the i-th unknown pixel intensity of the true object in *x-f* space. Equation 1 describes the aliased signal at location x for a single temporal frequency and is called the signal encoding equation of *k-t* BLAST (15). Since the single signal intensities of the true object are unknown, Eq. 1 is underdetermined. The challenge of a reconstruction algorithm is therefore to solve the signal encoding equation for an adequate representation of the true object from the aliased image pixels.To achieve this, the *k-t* BLAST technique implements a least squares method and incorporates an estimate of the signal covariance to optimize the reconstruction formalism. The aliased signal is then decomposed into the true object components according to their expected intensities:

$$\mathbf{P}_{\mathbf{xf}} = \mathbf{Cov}^2\mathbf{1}^{\mathbf{H}}(\mathbf{1} \cdot \mathbf{Cov}^2\mathbf{1}^{\mathbf{H}})^{-1}P_{\text{alias},x} \qquad [2]$$

The superscript -1 indicates the inverse, **H** the conjugate transpose and **1** the unity matrix. The estimate of the signal covariance matrix $\mathbf{Cov}^2$ is derived from an additional training data set that consists of a small number of central phase-encoding lines fully sampled over time, providing low spatial, but full temporal resolution (Fig. 1). By solving Eq. 2 for all aliased voxels the true object in the *x-f* domain can be reconstructed.

Note that the signal encoding equation in *k-t* BLAST remains underdetermined. The decomposition of the aliased signal into its true components depends solely on the low-resolution estimate of the signal covariance. This causes a rapidly increasing reconstruction error for increasing acceleration factors, resulting in reduced temporal fidelity accompanied by remaining aliasing artifacts. In general, the *k-t* BLAST method allows for minimal overlap of the object signal in the *x-f* domain. Nevertheless, if the signal overlap is stronger, as in the case of MR parameter mapping, the method is not sufficient to resolve all aliasing artifacts.

k-t PCA

The *k-t* PCA method is an extension of the *k-t* BLAST method. The full mathematical description can be found in the original publication by Pedersen et al. (16). In the following section, a brief review of the method is given. The idea behind *k-t* PCA is to employ more of the signal correlations inherent in the training data. As stated above the signals at different points in time are not independent of each other. Therefore, a standard compression technique, namely principal component analysis (PCA), can be used to find a matrix factorization of the data in the *x-f* domain that exploits this redundancy in such a way that the data are expressed in an uncorrelated and sparse manner in the so-called *x-pc* space (Fig. 2). In *k-t* PCA each temporal frequency profile of the training data in the *x-f* space is restated by a linear combination of a set of basis vectors (principle components). The advantage of this method is that the new basis expresses the main temporal features of the data with a minimum number of independent basis vectors. Therefore, it can be used to compress the data and reduce the number of degrees of freedom accordingly, in the reconstruction problem for undersampled data.

The main assumption of *k-t* PCA is that the temporal basis derived from the low resolution training data does not distinctly differ from the basis of the fully sampled *x-f* data. This means that the *x-f* data of the true object can be represented in the predetermined basis of the training data. Mathematically this can be expressed as follows:

$$P_{xf}(x, f_{\mathrm{m}}) = \sum_{i=1}^{n_{\mathrm{pc}}} \mathbf{P_{xpc}}(x, i) \cdot \mathbf{B}(i, f_{\mathrm{m}}) = \mathbf{p_{xpc}}(x) \cdot \mathbf{b}(f_{\mathrm{m}}) \quad [3]$$

where the rows of **B** contain the principal components (PCs) derived by applying the PCA to the training data in *x-f* space. The basis functions are the eigenvectors of the covariance matrix of the training data ordered according to their corresponding weighting coefficients (eigenvalues). The columns of the data in the new *x-pc* space, $\mathbf{P}_{\mathrm{xpc}}$, contain the temporally invariant weighting coefficients. The size of the weighting coefficients is a measure of the contribution of the corresponding principle components to the data variance. Most of the temporal dynamics within the data are typically modeled within the first few PCs. By restricting the sum in Eq. 3 and therefore the *x-pc* representation of the data to the first n_{pc} PCs, the corresponding *x-f* data can be represented in a much more compressed fashion. Based on Eq. 3 the signal encoding equation of *k-t* BLAST can be extended to

$$P_{\mathrm{alias}}(x, f_{\mathrm{m}}) = \mathbf{1B}_{\mathrm{m}}\mathbf{p}_{\mathrm{xpc}} \quad [4]$$

Here, $\mathbf{B}_{\mathrm{m}}$ and $\mathbf{p}_{\mathrm{xpc}}$ depict the corresponding columns and rows of **B** and $\mathbf{P}_{\mathrm{xpc}}$ of the aliased pixel. Similar to Eq. 1, the signal encoding equation for *k-t* PCA can be expressed for each frequency in *x-f* space as

$$\mathbf{P}_{\mathrm{alias},x} = \begin{bmatrix} P_{\mathrm{alias}}(x, f_1) \\ P_{\mathrm{alias}}(x, f_2) \\ \vdots \\ P_{\mathrm{alias}}(x, f_{n_{\mathrm{f}}}) \end{bmatrix} = \begin{bmatrix} \mathbf{1B_1} \\ \mathbf{1B_2} \\ \vdots \\ \mathbf{1B}_{n_{\mathrm{f}}} \end{bmatrix} \mathbf{p}_{\mathrm{xpc}} \equiv \mathbf{E}\mathbf{p}_{\mathrm{xpc}} \quad [5]$$

The data of the true object are now expressed in their matrix factorization in relation to the PCs. The signal encoding equation for *k-t* BLAST and *k-t* PCA become almost equivalent, if the matrix containing the basis functions **E**is replaced by the unity matrix **I,** which corresponds to the uncompressed original basis. The only difference is that the signal encoding equation for *k-t* PCA takes into account the aliasing for all temporal frequencies.

Analogous to Eq. 2, the solution to Eq. 5 is derived from the regularized least squares solution, this time based on the matrix expression of the new temporal basis vectors, **E**.

$$\mathbf{p}_{\mathrm{xpc}} = \mathbf{Cov_x^2 E^H}(\mathbf{E} \cdot \mathbf{Cov_x^2 E^H})^{-1}\mathbf{P_{alias,x}} \quad [6]$$

By solving Eq. 6 for all positions $\boldsymbol{x}$ of aliased voxels the true object in the *x-pc* domain is obtained. Finally, the reconstruction result is mapped back to the original basis in the *x-f* domain by the inverse PCA (Eq. 3). In a last step a Fourier transformation is applied to obtain the representation of the data in the time domain.

In contrast to the underdetermined *k-t* BLAST reconstruction problem, the signal encoding problem of *k-t* PCA can be overdetermined, if the number of measurements exceeds the number of unknown variables in the system. Image acquisition for *k-t* PCA consists of $n_x \times n_f/$ af measurements of phase encoding lines, where n_x is the number of phase encoding lines of a fully sampled image and n_f is the number of images over time. The data that are reconstructed in *x-pc* space consist of $n_x \times n_{pc}$ phase encoding lines, where n_{pc} is the number of applied PCs. Thus if the number of measurements for *k-t* PCA exceeds the amount of data that need to be reconstructed, that means if $n_{pc} < n_f/\mathrm{af}$, the reconstruction problem becomes overdetermined. In other words, the fewer PCs that are needed to adequately describe the dynamics of the true object, the more constrained and well-defined the reconstruction problem becomes.

METHODS

Data Acquisition

To investigate the performance of *k-t* PCA for fast MR parameter mapping, a standard segmented IR TrueFISP acquisition (10) was chosen for the quantification measurement allowing for a simultaneous extraction of the parameter maps for T_1, T_2 and relative spin density. The acquisitions consisted of non-slice selective adiabatic inversion pulses, 8 segments, 64 images along the relaxation curve, TR = 4.04 ms, flip angle= 50° and a matrix size of 192 × 192, Field-of-View (FOV) of 190 × 190 mm^2 and a slice thickness of 6 mm. Eight *k*-space segments were acquired to provide a fully encoded reference. The acquisition time per segment was 6 s. Between the acquisitions of each individual k-space segment a 10 s time delay was inserted to allow for full relaxation of the magnetization to thermal equilibrium. Thus the overall scan time for the fully sampled data was 2 min per slice. In the case of 8-fold undersampling, the delay could be removed and the scan time could be reduced to 6 s. A standard 12 channel head array was used as the signal receiver for the IR TrueFISP sequence.

In addition, an ECG-gated cardiac TrueFISP CINE data set with 21 phases per cardiac cycle was acquired as an example data set for dynamic imaging. A six channel body array in combination with six channels of a standard spine array was employed here.

All experiments were conducted on healthy volunteers, who gave written informed consent to participate in this study. All data sets were obtained in vivo on a MAGNETOM Avanto 1.5 T (Siemens Healthcare, Erlangen, Germany).

Application of *k-t* PCA

Data series were fully sampled over time. Undersampling was then performed retrospectively for varying acceleration factors (af = 2, 4, 8, 16) by selecting a smaller number of phase encoding lines in the *k*-space representation according to the sampling pattern in Fig. 1. The *k-t* PCA method was applied to the undersampled data and the outcome was later compared to the fully acquired data,

to directly measure *k-t* PCA performance. The suitable number of training data lines was tested by the reconstruction error for the different training profiles (1, 2, 4, 8, 16, 32, and 64 training data lines) with three basis functions and af = 8. Furthermore, the number of PCs was varied from 1 to 6, while the number of training data lines and the acceleration factor were kept constant (one single line in central *k*-space, af = 8). To compare the influence of different acceleration factors (af = 1, 2, 4, 8, 16), three PCs and one single training data line were used. Image quality was evaluated by the relative root mean square (RMS) error that was calculated for each test parameter as the RMS difference between the fully sampled data and the reconstructed images normalized by the RMS intensity of the fully sampled data.

Data Model

Finally, the *k-t* PCA reconstructed series of images of the IR TrueFISP measurement was fitted on a pixel-by-pixel basis to a three parameter mono-exponential model function proposed by Gulani and coworkers (10) to obtain the model parameters T_1*, INV and S_{stst}:

$$M(t) = S_{stst} \cdot \left[1 - \mathrm{INV} \cdot \exp\left(-\frac{t}{T_1^*}\right)\right] \quad [7]$$

The observed relaxation time value T_1* is a function of the true tissue parameters T_1 and T_2 and the flip angle. The inversion factor INV relates the signal value extrapolated to $t = 0$ and the steady state signal S_{stst}. It allows for the calculation of the ratio T_1/T_2. Thus, the parameter maps for T_1, T_2 and the relative spin density M_0 can be calculated pixelwise from the fitted parameters according to the following equations:

$$T_1 = T_1^* \cdot \left[\cos\frac{\alpha}{2} \cdot (\mathrm{INV} - 1)\right] \quad [8]$$

$$T_2 = T_1^* \cdot \left[\sin^2\frac{\alpha}{2} \cdot \left(1 - \frac{\cos\frac{\alpha}{2}}{\mathrm{INV} - 1}\right)^{-1}\right] \quad [9]$$

$$M_0 = S_{stst} \cdot \frac{(\mathrm{INV} - 1)}{\sin\frac{\alpha}{2}} \quad [10]$$

It is assumed in Eqs. 8–10 that the magnetization reaches its thermal equilibrium before the next inversion starts. Due to the finite wait time of 10s between the segments, this was not the case in our study resulting in a systematic underestimation of M_0. We corrected for this effect as described in the Appendix of Gulani et al. (11)

$$M_0 = \frac{M_{eff} - S_{stst}\left[1 - \mathrm{INV} \cdot \exp\left(-\frac{t_{scan}}{T_1}\right)\right] \cdot \cot\left(\frac{\alpha}{2}\right) \cdot \exp\left(-\frac{t_{wait}}{T_1}\right)}{1 - \exp\left(-\frac{t_{wait}}{T_1}\right)} \quad [11]$$

where t_{scan} is the time at the end of the sampled relaxation curve and t_{wait} is the wait time after sampling when the longitudinal component of the relative spin density relaxes along the *z*-axis to its effective value after wait time, M_{eff}. We further used the corrected M_0 value to adjust T_1 and T_2. All corrections had only an effect on extremely long T_1 and T_2 times, as they can be found in CSF. Finally, the receiver coil sensitivity profiles where measured and used to normalize the intensity of the M_0 maps. Thus, the derived maps directly reflect the relative spin density. Further correction factors accounting e.g., for B_1, B_0 and temperature would additionally need to be applied to yield quantitative spin density maps (6).

RESULTS

Modification of *k-t* PCA

Basis Vectors for Dynamic and Relaxation Data

An overview of the representation of the acquired dynamic and relaxation data in various image domains is provided in Fig. 3. The fully sampled MR parameter data show a broad extension in the *x-f* domain, leading to a strong signal overlap in the case of undersampling. In contrast, the dynamic data are sparsely represented in *x-f* space, with little signal overlap for undersampled image acquisition. On the other hand, if the data are transformed into their *x-pc* representation via PCA, the appearance is reversed. The dynamic data are more expanded than the relaxation data. The location beyond which the normalized weighting coefficients are close to zero (smaller than 1 ppm of the biggest weighting coefficient) is indicated by a white dashed line (Fig. 3, right panel). The additional subplot shows the intensity of the weighting coefficients of the PCs for a particular location. As seen in Fig. 3, the main variance of the MR parameter quantification data is accurately encoded with three PCs, whereas ~11 PCs contribute significantly to the temporal variance in the dynamic cardiac data. Figure 4 shows the influence of the number of basis functions (from 1 to 6 PCs) on the overall image quality of the reconstructed MR parameter quantification data. The relative RMS error remains low for two and three PCs. Adding an extra PC merely adds noise to the reconstruction because of the low corresponding weighting coefficient. This causes an increase in the relative RMS error of 32% from three to four PCs (Fig. 4a).

Number of Training Data Lines

Figure 4b depicts the influence of the number of training data lines in central *k*-space on the reconstruction performance. We measured a slight increase in the relative RMS error for a larger number of training data lines (10% error increase for 64 compared to one training data line). Additionally the quality of the image series did not significantly depend on the number of training data lines used for reconstruction. Hence for further investigations only a single line in central *k*-space was used as training data.

Acceleration Factor

As expected, the overall relative RMS error of the MR parameter reconstruction increased for larger acceleration factors. Figure 4c shows the increase of 0.2% from 2- to 4-fold acceleration and a further increase of 7.2% for 8-fold

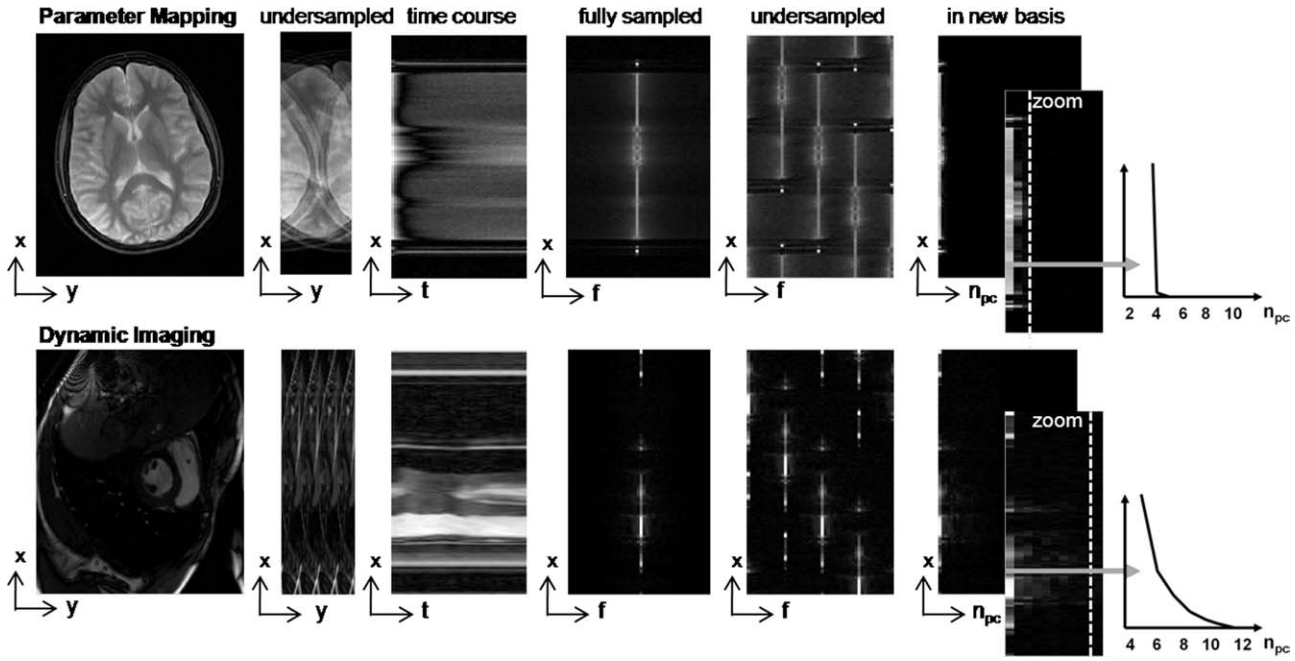

FIG. 3. In vivo measurements: Comparison of the different image spaces involved in *k-t* PCA for MR parameter mapping (top) and dynamic CINE data (down). From left to right: fully sampled data, 4-fold undersampled data, time course of the fully sampled data, representation of fully sampled and 4-fold undersampled data in the frequency domain, transformed data after PCA in the *x-pc* domain and enlargement of the *x-pc* representation. Additionally a particular line at location *x* in *x-pc* representation is plotted for each data set. The ordinate corresponds to the signal intensity of the weighting coefficients. The abscissa represents the number of PCs. The part in the *x-pc* space location, beyond which the normalized weighting coefficients are close to zero (smaller than 1 ppm of the biggest weighting coefficient) is indicated by a white dashed line (right panel).

acceleration. The reconstruction performance becomes insufficient for acceleration factors beyond af = 8, mainly due to a strong amplification of the noise level in the first few images of the time series at higher accelerations. The first image of the time series already exhibits a decrease in the signal-to-noise-ratio (SNR) of 5.6 % from 2- to 4-fold acceleration and a decrease of 13.9% from 4- to 8-fold acceleration. Later images in the time series showed only moderate SNR differences for varying acceleration factors (∼2%). Figure 5 depicts an overview of the image quality of the first 4 images and the time course of each image series for 1, 2, 4 and 8-fold acceleration. The increased noise level becomes evident in the zoom-in of the fully sampled data and 8 fold acceleration.

General Method Performance

Figure 6 depicts the parameter maps of the MR parameters for different acceleration factors (af = 2, 4, 8) in comparison to the fully sampled data (af =1). No remaining aliasing artifacts can be observed for the accelerated data. Regions of interest (ROIs) were placed at various locations, e.g., in frontal and occipital white matter, gray matter, thalamus, CSF, putamen and caudate nucleus, in the fully sampled and accelerated data. The mean voxel intensities of the ROIs were compared for T_1 and T_2 parameter maps of the reconstructed data and the fully sampled data (Fig. 7). Little variation compared to the fully encoded gold-standard can be observed for different

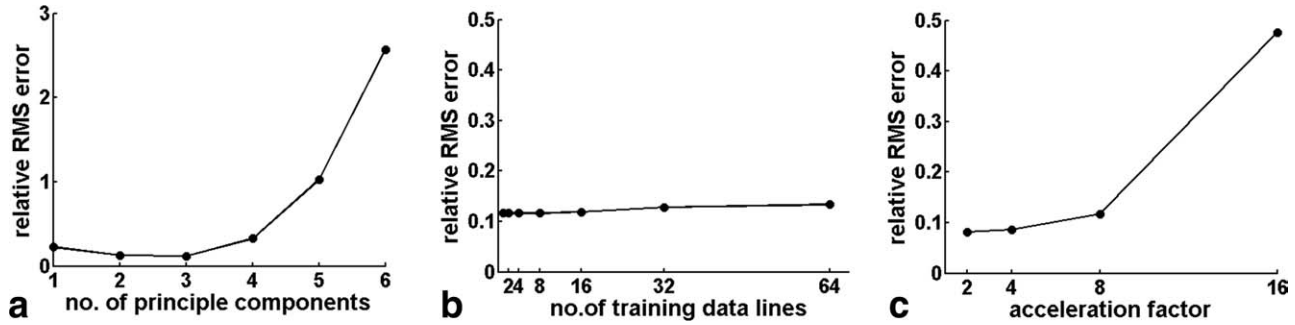

FIG. 4. Relative RMS error of the reconstructed data compared to the fully sampled data of the quantification measurement for different changes in the configuration of the *k-t* PCA parameters. **a:** Relative RMS error for varying numbers of PCs (af = 8, 1 training data line). **b:** Relative RMS error for varying numbers of training data lines (af = 8, 3 PCs). **c:** Relative RMS error for varying acceleration factors (three PCs, one training data line).

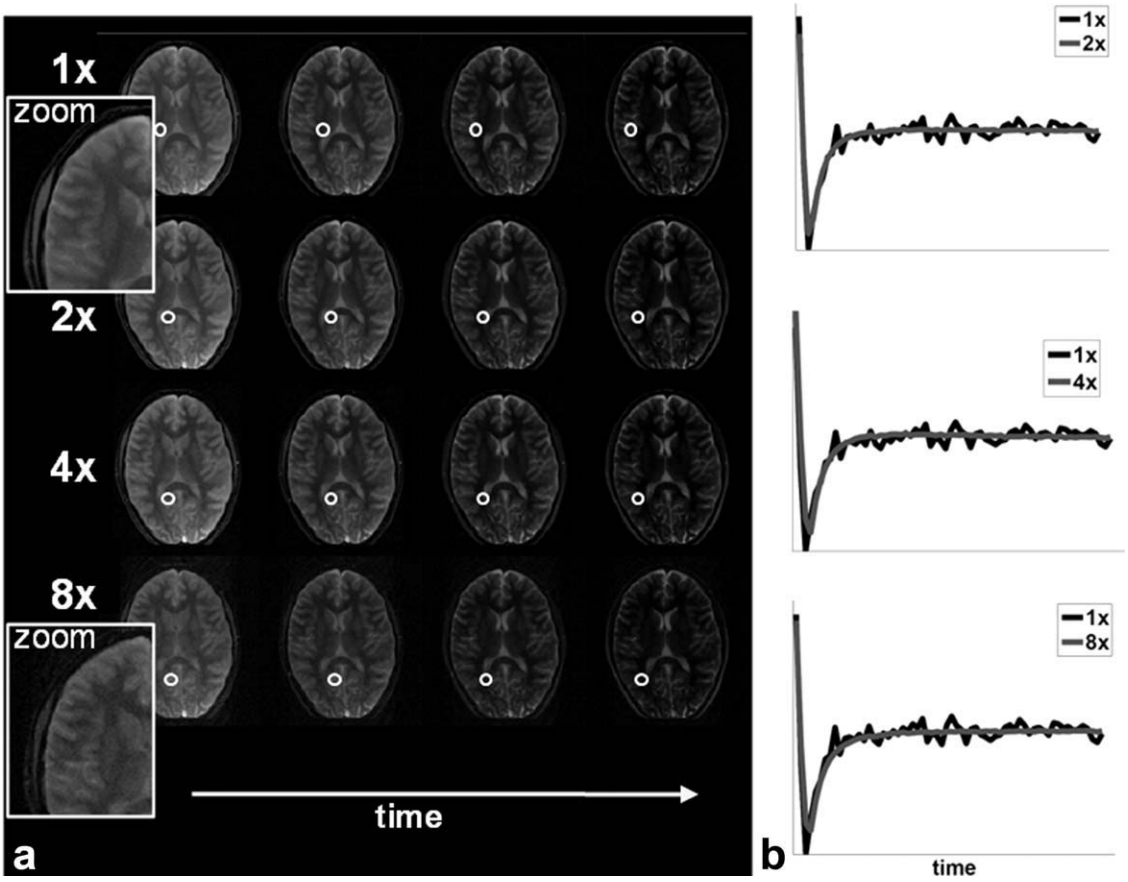

FIG. 5. Image series over time for fully sampled and accelerated data. **a:** First four images for the time series of the fully sampled (1×) and reconstructed data (2, 4, 8× acceleration, 3 PCs, 1 training data line). A zoom-out of the first image for 8-fold acceleration and fully sampled data is displayed. **b:** The time series for each acceleration factor (gray) is plotted for a single pixel indicated in (a) by a white circle compared to the original time series (black).

T_1 and T_2 values; all parameter values obtained from the reconstructed data match the fully sampled data within the bounds of the error.

In addition, the mean intensities for the fully sampled and 8-fold accelerated data were compared to standard values reported in the literature for the particular region (6,8,10). All values are listed in Table 1. In general, the parameters of the accelerated measurement and the fully acquired data match the reference values within the bounds of the error. The only exception is the T_2 value for CSF that does not match the reference value reported in the literature for an IR TrueFISP measurement (10). The standard deviation for the reconstructed data is consistently larger for the 8-fold accelerated data compared to the fully sampled data.

DISCUSSION

Modification of *k-t* PCA

Basis for Dynamic and Relaxation Data

The *k-t* PCA method is based on a transformation of the data into a new set of basis functions that are tailored to their temporal dynamics. We found a minimum of 11 basis functions that significantly contribute to the signal time course of the cardiac CINE experiment. This result is in accordance with the findings of a previous study by Pedersen et al. where an optimal number of around 10 basis functions was reported (16). In addition, this study demonstrates that only three basis functions were required to encode the dynamics of an MR parameter mapping IR TrueFISP experiment. We ascribe this finding to the simple temporal dynamics of MR parameter mapping. Fundamentally an exponential time course underlies all signal intensities over time in MR parameter mapping; the exact shape of the curve is spatially dependent and thus determined by the weighting coefficients, but the general dynamic remains very similar and can be described by 2–3 basis functions.

Furthermore, the number of basis functions determines the maximal compression rate of the data and thus, the number of degrees of freedom in the reconstruction method. A high number of PCs causes an underdetermined reconstruction problem for *k-t* PCA, in which the signal estimate will more strongly rely on the estimated signal covariance and thus, become more similar to *k-t* BLAST. In the case of MR parameter mapping, this will cause strong residual aliasing artifacts. Additional PCs, which do not encode the true temporal dynamics, mainly encode variance in the data that is due to noise. This can be observed in Fig. 5b were the

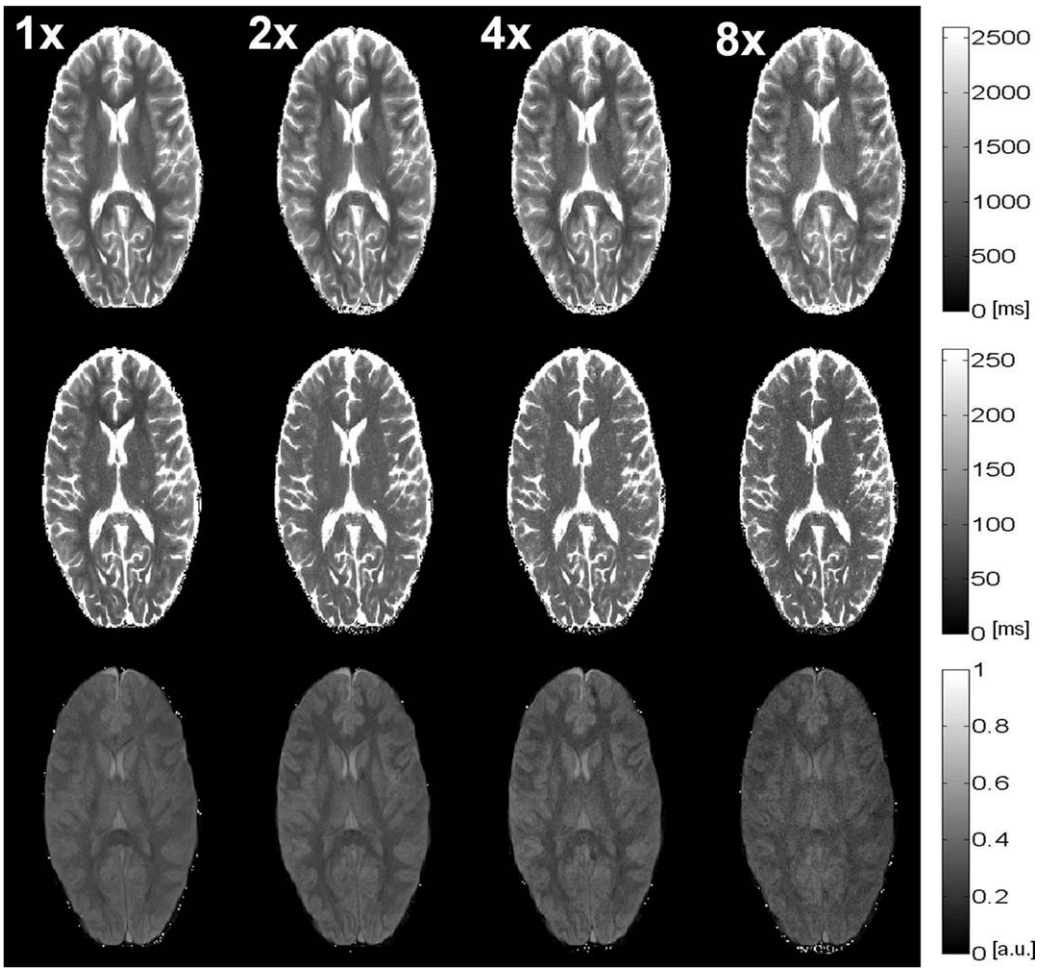

FIG. 6. MR parameter maps for T_1, T_2 and relative spin density for the fully sampled data (left) and the undersampled data and with *k-t* PCA reconstructed data (from left to right: 1, 2, 4, and 8-fold acceleration, three PCs, one training data line).

time curves of the reconstructed data with few PCs appear to be smoothed compared to the original data. Adding these low variance components will lead to an increased noise level in the reconstruction and an increase in the relative RMS error (Fig. 4). On the other hand, if the number of PCs is too small, the time course of the data is not sufficiently described by the PCs leading to a systematically wrong shape of the relaxation curves also causing an increase in the relative RMS error. Thus, an optimal number of basis functions always exists, which is strongly dependent on the temporal dynamics of the measurement. For relaxation data, this value will most likely vary between 2 and 4 basis functions.

Number of Training Data Lines

The number of training data lines plays a crucial role in the maximal achievable acceleration factor for *k-t* PCA. The optimal number of training data lines reported for cardiac imaging with *k-t* BLAST/*k-t* PCA is in the range of 10 to 20 (16–19). Pedersen et al. used a convention of 11 training data lines for *k-t* PCA in cardiac imaging (16). In contrast to previous findings for dynamic data, we showed that for the reconstruction of quantitative data a single training data line in central *k*-space is sufficient to reconstruct the MR parameters from an IR TrueFISP measurement. Furthermore, a larger number of training data lines did not improve the reconstruction quality. This result can be attributed to the fact that a single line in central *k*-space encodes the main temporal dynamics independent of the spatial resolution, since all voxels exhibit an exponential decay with varying shape. In contrast, in dynamic imaging various strongly differing time courses are possible. Thus, depending on the voxel location, additional temporal components need to be encoded. This finding allows for a combined sampling pattern for training and undersampled data and an additional reduction in acquisition time for MR parameter mapping. Furthermore, it proves that the amount of required training data is strongly dependent on the complexity of the dynamics.

Acceleration Factor

The maximal achievable acceleration factor for the IR TrueFISP was found to be eight. Consistent with the findings of Pedersen et al. (16) the accuracy for *k-t* PCA for larger acceleration factors e.g., af = 16 falls below a clinically acceptable level. However, this is certainly

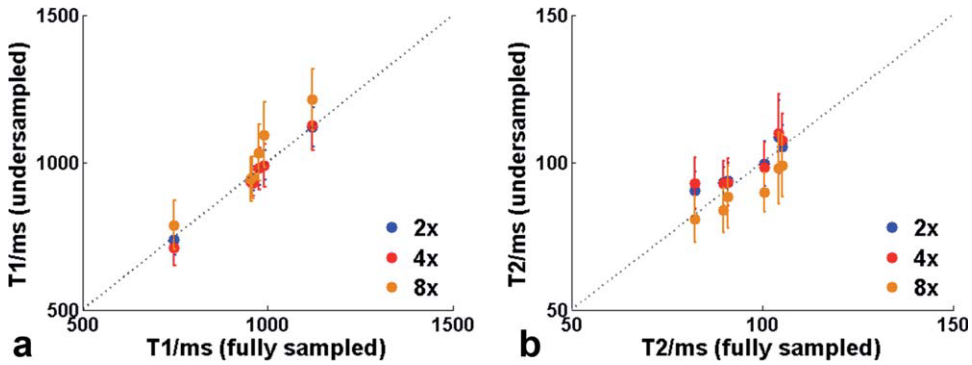

FIG. 7. Correlation between relaxation times obtained from the fully sampled (abscissa) and the undersampled and reconstructed in vivo data (ordinate) for the 2-fold (blue), 4-fold (red), and 8-fold (orange) acceleration (three PCs, one training data line) in different ROIs in the brain, including white matter, gray matter and putamen. The dotted slope indicates where both relaxation values are identical. **a:** demonstrates the comparison for various T_1, (**b**) for T_2 values.

dependent on the SNR of the measurement, the number of acquired images per time series and the possible compression rate given by the number of PCs.

General Method Performance

We demonstrated that a simultaneous measurement of T_1, T_2 and relative spin density with an IR TrueFISP sequence can be significantly accelerated using *k-t* PCA. Furthermore, the acquisition time of the measurement can be shortened due to the small amount of required training data. Thereby the parameter values up to an acceleration factor of eight agreed well with the literature values.

Limitations

One major limitation of the method is noise level in the reconstructed data. A significant SNR decrease can be observed solely for the first few images of the time series for larger acceleration factors. One reason is expected to be the matrix inversion implemented in the *k-t* PCA reconstruction.

In contrast to the *g*-factor related spatially dependent noise enhancement typically observed in parallel MRI in SENSE (20) and GRAPPA (21) reconstructions, the noise enhancement observed here features a strong temporal variation, especially for high acceleration factors and higher numbers of PCs. In this study, this led to maximum acceleration factor of eight. Given that IR TrueFISP measurements have a relatively high SNR, this effect might become a severe problem for a further application of *k-t* PCA on sequences with low SNR.

Furthermore, there are sources of error in the estimation of the MR parameters. First we assume the relaxation process to be mono-exponential. Yet this is an approximation. Due to multiple compartments of different tissues within a single voxel, the relaxation behavior is multi-exponential. More accurate results on the parameter values could be achieved by fitting a multi-exponential decay with no assumptions about the number of exponential components (22). Moreover, most *k*-space lines are acquired when relaxation was nearly complete, only a few lines are acquired on the steep relaxation slope right after the inversion pulse. This results in a slight blurring of the first few images for short T_1 values compared to the later images of the series. However, we were able to weaken this effect by an 8-fold segmentation of the sequence allowing for an inter-image time delay of only 100 ms at a TR of 4ms.

In addition, the parameter quantification with IR TrueFISP is subject to some systematic errors originating mainly from the discrepancy between the experimentally and theoretically derived signals for steady state free precession (SSFP) sequences. One cause of inaccuracy in the parameter estimation is that the finite radio frequency (RF) pulses lead to an increase of the steady state signal intensity due to T_1 relaxation during the pulses. Thus, a correction of SSFP sequences was suggested for quantitative measurements (23,24). In addition, latest studies

Table 1
Average ± Standard Deviation of T_1 and T_2 Relaxation Times in Particular ROIs in the Brain for Fully Sampled and 8-Fold Accelerated Data (First and Second Column) Compared with Reference Values in the Literature (Third Column)

	T_1/ms			T_2/ms		
	1×	8×	Lit.	1×	8×	Lit.
White matter	748 ± 34	770 ± 93	719 ± 33 (10)	70 ± 7	80 ± 12	73 ± 6 (10)
						78 ± 3 (6)
Gray matter	955 ± 41	943 ± 75	1165 ± 88 (10)	104 ± 10	99 ± 10	92 ± 11 (10)
			1065 ± 98 (8)			98 ± 7 (8)
			1048 ± 61 (6)			94 ± 6 (6)
CSF	3715 ± 459	3853 ± 512	3337 ±111 (10)	1120 ± 391	1052 ± 818	2562 ± 123 (10)
			3940 ± 340 (6)			1910 ± 520 (6)

found a systematic overestimation of T_1 that is thought to be due to the influence of magnetization transfer on a SSFP signal (23,25). Furthermore, additional deviations of the estimated MR parameter from the true tissue parameters can be caused by the strong dependency of MR parameters on the flip angle used in an IR TrueFISP measurement, especially for T_2. Thus, deviations of the observed relaxation values in T_2 compared to the reference can be caused by a suboptimal excitation slice profile in our sequence and may result in errors in T_2 up to 40%. This effect can either be minimized by improving the slice profile of the pulse (i.e., higher time-bandwidth product, leading to higher RF deposition) or completely removed by using 3D sequences with an optimal slab profile; however, deviations arising from potential B_1 inhomgeneties remain. While B_1 field homogeneities can be reduced to a minimum at 1.5T by employing the system body-coil for transmission and a receive-only phased array head coil for signal reception, as used in our setup, strong effects can be expected at higher fields and when local transmit coils are used (26).

These limitations mainly affect the accuracy of the estimated parameters. Nevertheless a further improvement of the IR TrueFISP sequence is expected to have no effect on our general finding that the *k-t* PCA method is capable of significantly accelerating parameter quantification measurements.

Applications

The true value of our findings is that *k-t* PCA is applicable to a variety of acquisition techniques where a series of images is acquired. It has already shown to improve the accuracy of accelerated dynamic imaging (16) and we further investigated the application on simultaneous MR parameter quantification using IR TrueFISP in this study. Another potential application could be contrast-enhanced perfusion imaging or MR Angiography. The performance of *k-t* PCA is strongly dependent on the number of degrees of freedoms in the reconstruction. Thus, time series with even simpler temporal dynamics will further benefit from the method as shown for a modified IR TrueFISP sequence (27,28).

It is expected that an extension to 3D imaging enables quantification of the whole brain with an IR TrueFISP measurement and 1.4 mm isotropic resolution in about 6 min (25). Further acquisition time reduction could also be achieved by using predetermined basis functions from simulated artificial relaxation data and therefore without the need of the acquisition of extra training data. A combination with other fast quantification imaging techniques such as QRAPMASTER (6) is also feasible. Thereby the advantage of *k-t* PCA compared to other reconstruction concepts presented for fast MR parameter mapping is the low computational cost to calculate the reconstructed data (29) and the small amount of training data required.

CONCLUSION

The *k-t* PCA concept was successfully applied to significantly accelerate the acquisition of the IR TrueFISP sequence for simultaneous quantification of T_1, T_2 and relative spin density. Owing to the simple temporal dynamics of the time course, the relaxation data can be expressed by a very small number of basis functions. This allows for an extremely constrained reconstruction and up to 8-fold accelerated acquisition. Furthermore, the amount of training data can be restricted to a single line in central *k*-space. These findings in combination with the flexibility of the method make *k-t* PCA a potential technique to bring the acquisition time for MR parameter mapping to a clinically acceptable level.

ACKNOWLEDGMENTS

The authors acknowledge Philipp Ehses for the scientific support.

REFERENCES

1. Bottomley PA, Hardy CJ, Argersinger RE, Allen-Moore G. A review of 1H nuclear magnetic resonance relaxation in pathology: are T1 and T2 diagnostic? Med Phys 1987;14:1–37.
2. Tofts P. Quantitative MRI of the brain: measuring change caused by disease. Chichester: Wiley; 2003.
3. Vymazal J, Righini A, Brooks RA, Canesi M, Mariani C, Leonardi M, Pezzoli G. T1 and T2 in the brain of healthy subjects, patients with Parkinson disease, and patients with multiple system atrophy: relation to iron content. Radiology 1999;211:489–495.
4. Odrobina EE, Lam TY, Pun T, Midha R, Stanisz GJ. MR properties of excised neural tissue following experimentally induced demyelination. NMR Biomed 2005;18:277–284.
5. Zipp F. A new window in multiple sclerosis pathology: non-conventional quantitative magnetic resonance imaging outcomes. J Neurol Sci 2009;287(Suppl 1):S24–29.
6. Warntjes JB, Leinhard OD, West J, Lundberg P. Rapid magnetic resonance quantification on the brain: optimization for clinical usage. Magn Reson Med 2008;60:320–329.
7. Preibisch C, Deichmann R. T1 mapping using spoiled FLASH-EPI hybrid sequences and varying flip angles. Magn Reson Med 2009;62: 240–246.
8. Deoni SC, Peters TM, Rutt BK. High-resolution T1 and T2 mapping of the brain in a clinically acceptable time with DESPOT1 and DESPOT2. Magn Reson Med 2005;53:237–241.
9. Warntjes JB, Dahlqvist O, Lundberg P. Novel method for rapid, simultaneous T1, T_2*, and proton density quantification. Magn Reson Med 2007;57:528–537.
10. Schmitt P, Griswold MA, Jakob PM, Kotas M, Gulani V, Flentje M, Haase A. Inversion recovery TrueFISP: quantification of T(1), T(2), and spin density. Magn Reson Med 2004;51:661–667.
11. Gulani V, Schmitt P, Griswold MA, Webb AG, Jakob PM. Towards a single-sequence neurologic magnetic resonance imaging examination: multiple-contrast images from an IR TrueFISP experiment. Invest Radiol 2004;39:767–774.
12. Kellman P, Epstein FH, McVeigh ER. Adaptive sensitivity encoding incorporating temporal filtering (TSENSE). Magn Reson Med 2001; 45:846–852.
13. Breuer FA, Kellman P, Griswold MA, Jakob PM. Dynamic autocalibrated parallel imaging using temporal GRAPPA (TGRAPPA). Magn Reson Med 2005;53:981–985.
14. Huang F, Akao J, Vijayakumar S, Duensing GR, Limkeman M. k-t GRAPPA: a k-space implementation for dynamic MRI with high reduction factor. Magn Reson Med 2005;54:1172–1184.
15. Tsao J, Boesiger P, Pruessmann KP. k-t BLAST and k-t SENSE: dynamic MRI with high frame rate exploiting spatiotemporal correlations. Magn Reson Med 2003;50:1031–1042.
16. Pedersen H, Kozerke S, Ringgaard S, Nehrke K, Kim WY. k-t PCA: temporally constrained k-t BLAST reconstruction using principal component analysis. Magn Reson Med 2009;62:706–716.
17. Plein S, Ryf S, Schwitter J, Radjenovic A, Boesiger P, Kozerke S. Dynamic contrast-enhanced myocardial perfusion MRI accelerated with k-t sense. Magn Reson Med 2007;58:777–785.

18. Baltes C, Kozerke S, Hansen MS, Pruessmann KP, Tsao J, Boesiger P. Considerations on training data in k-t BLAST/k-t SENSE accelerated quantitative flow measurements. Proc Intl Soc Magn Reson Med 2005;13:383.
19. Hansen MS, Kozerke S, Pruessmann KP, Boesiger P, Pedersen EM, Tsao J. On the influence of training data quality in k-t BLAST reconstruction. Magn Reson Med 2004;52:1175–1183.
20. Pruessmann KP, Weiger M, Scheidegger MB, Boesiger P. SENSE: sensitivity encoding for fast MRI. Magn Reson Med 1999;42: 952–962.
21. Breuer FA, Kannengiesser SA, Blaimer M, Seiberlich N, Jakob PM, Griswold MA. General formulation for quantitative G-factor calculation in GRAPPA reconstructions. Magn Reson Med 2009;62:739–746.
22. MacKay A, Laule C, Vavasour I, Bjarnason T, Kolind S, Madler B. Insights into brain microstructure from the T2 distribution. Magn Reson Imaging 2006;24:515–525.
23. Bieri O, Scheffler K. SSFP signal with finite RF pulses. Magn Reson Med 2009;62:1232–1241.
24. Crooijmans HJ, Gloor M, Bieri O, Scheffler K. Influence of MT effects on T(2) quantification with 3D balanced steady-state free precession imaging. Magn Reson Med 2011;65:195–201.
25. Ehses P, Gulani V, Yutzy S, Seiberlich N, Jakob PM, Griswold MA. Single-shot proton density, T1 and T2 quantification with radial IR TrueFISP: effect of magnetization transfer and long RF pulses. Proc Intl Soc Mag Reson Med 2010;18:2969.
26. Newbould R, Bammer R. Flip angle sensitivity in IR-trueFISP T1 and T2 mapping. Proc Intl Soc Mag Reson Med 2005;13:2191.
27. Petzschner FH, Ponce IPG, Blaimer M, Jakob PM, Breuer FA. Fast MR parameter mapping using k-t PCA. Proc Intl Soc Mag Reson Med 2010;18:544.
28. Breuer F, Darji N, Ehses P, Jakob PM, Blaimer M. Rapid high-resolution relaxation time and spin-density quantification using a modified segmented IR-trueFISP sequence. Proc Eur Soc Mag Reson Med Biol 2009;25:183.
29. Doneva M, Senegas J, Börnert P, Eggers H, Mertins A. Accelerated MR parameter mapping using compressed sensing with model-based sparsifiying transform. Proc Intl Soc Mag Reson Med 2009;17:385.